Int. J. Electrochem. Sci., 9 **(2014)** 7629 - 7643

International Journal of
ELECTROCHEMICAL
SCIENCE
www.electrochemsci.org

Electrochemical Fabrication and Thermoelectric Performance of the PEDOT:PSS Electrode Based Bilayered Organic Nanofilms

Hui Shi[†], *Congcong Liu*[†], *Jingkun Xu*[*], *Haijun Song, Qinglin Jiang, Baoyang Lu, Weiqiang Zhou, Fengxing Jiang*

Jiangxi Key Laboratory of Organic Chemistry, Jiangxi Science and Technology Normal University, Nanchang 330013, PR China
[*]E-mail: xujingkun@tsinghua.org.cn
†These authors contribute to this work equally

Received: 31 August 2014 / *Accepted:* 29 September 2014 / *Published:* 28 October 2014

A novel generation of PEDOT:PSS/PPY and PEDOT:PSS/PANI bilayered nanofilms were successfully prepared by electrochemical polymerization in a mixed alcohol solution of isopropyl alcohol (IPA), boron trifluoride ethyl ether (BFEE), and polyethylene glycol (PEG), based on a PEDOT:PSS nanofilm electrode. The structure, electrochemical, optical, and morphology of the as-formed films were systematically investigated by FT-IR, cyclic voltammetry (CV), UV−vis, and SEM. Thermoelectric (TE) investigations revealed that the electrical conductivity of the films was increased with the increasing BFEE proportion, and the values for PEDOT:PSS/PPY and PEDOT:PSS/PANI were 97.1 and 212.6 S cm^{-1} in the case of 30% BFEE. Meanwhile, the Seebeck coefficient kept at a relative high and stable level, with the maximum value of 23.3 μV K^{-1} for PEDOT:PSS/PPY and 27.8 μV K^{-1} for PEDOT:PSS/PANI. It was encouraging that the power factor of PEDOT:PSS/PANI films could reach up to be 12.0 μW m^{-1} K^{-2}, obtaining the maximum *ZT* value of 2.12×10^{-2} by estimates. Furthermore, as a new-found set of pure organic bilayered nanostructure materials, they may possess a great potential for realizing wide applications in TE or other organic electronics fields.

Keywords: PEDOT:PSS, Polypyrrole, Polyaniline, Electrochemical, Thermoelectric

1. INTRODUCTION

Thermoelectric (TE) materials and systems have focused great research interest in recent years, in particular because they can realize a direct conversion between thermal energy and electrical energy upon applying a thermal gradient to the materials [1]. Generally, the efficiency of TE materials can be evaluated by a dimensionless figure of merit, $ZT = S^2\sigma T/\kappa$, where *S* stands for the Seebeck coefficient,

σ and κ are the electrical and thermal conductivities, and T is the absolute temperature. Among the various categories of TE materials, a great deal of attention has recently been given to the conducting polymers, due to their potentially low cost, scalable manufacturing, and inherently low thermal conductivity [2].

Currently, the exploration of obtaining flexible TE materials with high figure of merit is meaningful and challengeable. Nanostructuring has been proposed to be one of the most effective and practical strategies in realizing high *ZT* values, due to the occurrence of the quantum confinement effects that increases the local density of states near the Fermi level [3,4]. Bubnova et al. and Kim et al. have reported the attractive TE performance of PEDOT nanofilms [5,6]. In addition, it is considered that ordered structures, for example, multilayered structure, also beneficial for improving the TE properties. High-quality multilayer structures of Al-doped ZnO, In and Al co-doped ZnO layers have been deposited using RF sputtering. Experimental and theoretical calculations have been conducted to systematically investigate their TE performance, and the maximum Seebeck coefficient was 1000 μV K^{-1} at 700 ^{o}C [7]. Then, Song and co-workers have obtained remarkably enhanced electrical conductivity and Seebeck coefficient by preparing layered PEDOT:PSS/SWCNTs nanocomposite, and the calculated power factor value was as high as 21.1 μW m^{-1} K^{-2} [8].

The typical conducting polymers of polypyrrole (PPY), polyaniline (PANI), polythiophene (PTh) and their respective derivatives, which show interesting optical and electrical properties, are playing an increasingly important part in a diverse range of applications as supercapacitors, transistors, solar cells, and light-emitting diodes [9−12]. Maddison and Yakuphanoglu have respectively investigated the TE properties of PPY and PANI films [13,14]. Yao et al. have prepared the PANI/SWCNTs composite films, where enhanced electrical conductivity and Seebeck coefficient were obtained [15]. It was worth mentioning that Toshima prepared the multilayered films composed of insulating and conductive PANI, exhibiting six times higher *ZT* value [2]. Furthermore, there have been a vast number of researches studying the conductivity mechanism of conducting polymers, and indicated that the electrical conductivity follows a quasi one-dimensional (1D) variable range hopping (VRH) model [16−19].

Ouyang and co-workers have systematically reported that an enhancement in the electrical conductivity of PEDOT:PSS could be obtained by adding different organic compounds called secondary dopants or additives [20,21]. Groenendaal et al. also indicated that the PEDOT:PSS films could be heated in air at 100 ^{o}C for over 1000 h with only a minimal change in conductivity [22]. Accordingly, the high-conductive and stable PEDOT:PSS thin films are very promising to be the electrode materials [21,23]. In our previous work, PEDOT:PSS nanofilms were put forward for the first time as the working electrodes to electrodeposit other polymer films of PTh and its derivatives [24] However, unlike thiophene and its derivatives, monomers of pyrrole and aniline are unstable in pure BFEE solution. Xu et al. have firstly put forward the mixed alcohol solution of isopropyl alcohol (IPA), boron trifluoride ethyl ether (BFEE), and polyethylene glycol (PEG) for the electropolymerization of pyrrole, and the films exhibited improved electrical conductivity [25].

In the present work, we described the successful preparation of the PEDOT:PSS/PPY and PEDOT:PSS/PANI bilayered nanofilms in virtue of easy electrochemical polymerization performed in a mixed alcohol solution of IPA, BFEE, and PEG, based on the high-conductive PEDOT:PSS nanofilm

electrodes. The TE performance and structures of the as-formed nanofilms have been systematically investigated.

2. EXPERIMENTAL DETAILS

2.1 Materials

PEDOT:PSS aqueous solution (PH1000; Baytron), pyrrole (98%; J&K Chemical Ltd), aniline (99.5%; J&K Chemical Ltd), DMSO (analytical grade; Beijing Chemical Works), were used directly as received. BFEE (Beijing Changyang Chemical Plant) was purified by distillation and stored at −20 ^{o}C before use.

2.2 Preparation of the bilayered nanofilms

Firstly, PEDOT:PSS/5% DMSO (herein referred to as PEDOT:PSS) nanofilms was prepared by spin-coating at speed of 2000 r min^{-1}.

Then, the spin-coated PEDOT:PSS-glass connected to wire in virtue of silver paint was used as the working electrode in a three-electrode cell configuration for the electropolymerization of pyrrole and aniline. Ag/AgCl and stainless steel sheets were used as the reference and counter electrode, respectively. 0.025 M pyrrole or 0.05 M aniline monomer was mixed in electrolyte solvent of IPA, 10%~30% (by volume) BFEE, and 5% PEG. All solutions were deaerated by bubbling argon gas and were maintained at a low overpressure during the polymerization process. All electropolymerization experiments were performed at the room temperature.

Detailed preparation process and the structures of the bilayered nanofilms are presented in Schema 1.

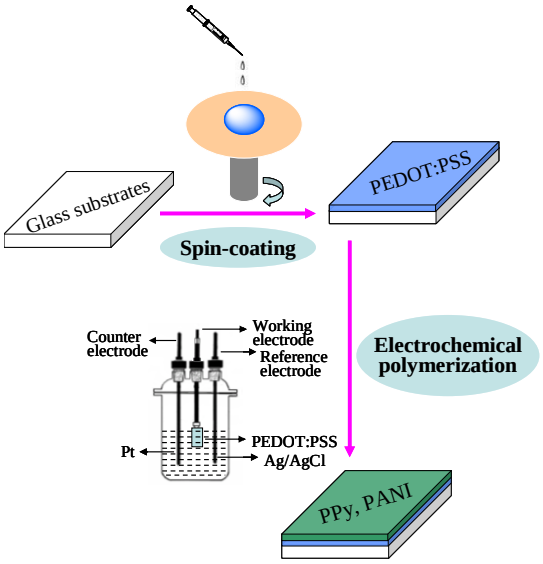

Scheme 1. Schematic diagram of the preparation of bilayered nanostructure films

2.3 Characterizations

The electropolymerization was conducted by a Model 263 potentiostat/galvanostat (EG&G Princeton Applied Research, Oakridge, TN) under the control of a computer. The thickness was measured with a Filmetrics F20 thin-film analyzer. FT-IR spectra were carried out using a Bruker Vertex 70 Fourier Transform Infrared Spectrometer. UV-vis absorption spectra were conducted by a Perkin-Elmer Lambda 900 UV-vis-near-infrared (NIR) spectrophotometer. SEM measurements were performed with a JEOL JSM-6701F field emission scanning electron microscope. HMS-3000 was used to determine the carrier mobility and carrier concentration.

Before the TE measurements, samples of PEDOT:PSS, PEDOT:PSS/PPY, and PEDOT:PSS/PANI nanofilms were cut into rectangular shape (length, 20.0 mm; width, 5.0 mm) and suspended by using a thermal paste between two thermoelectric devices (typically about 20 mm apart) used for creating a temperature difference. Electrical conductivity was measured by a four-point probe apparatus along with a Keithley 2700 Multimeter (Cleveland, OH) in conjunction with the Labview (National Instruments, Austin, TX) after four metal lines were patterned with silver paint. For the Seebeck coefficient measurement, a Keithley 2700 Multimeter (Cleveland, OH) and a regulated DC power supply (MCH-303D- II China) in conjunction with the Labview (National Instruments, Austin, TX) were utilized. Temperature gradients along the long edge of the sample were measured by two T-type thermocouples. Similar method has been reported by Kim et al. [26] Liquid nitrogen was used to provide the low temperature measurement. For electrical conductivity test, the temperature range is 300–100 K, and the steppes temperature is about 1 K min^{-1}. While for the Seebeck coefficient measurement, the temperature range is 300–250 K, and the steppes temperature is 0.3 K min^{-1}.

3. RESULTS AND DISCUSSION

Fig. 1 shows the anodic polarization curves of pyrrole and aniline in a mixed system of IPA, 10~30% BFEE, and 5% PEG. The onset oxidation potential of pyrrole was 0.62, 0.59, and 0.54 V on condition of 10%, 20%, 30% BFEE (Fig. 1a−c). While that of aniline with BFEE content of 10%, 20%, and 30% was 0.93, 0.87, and 0.82 V, respectively (Fig. 1d−f). The results demonstrate that the onset oxidation appears a trend of decline, along with the increasing BFEE content, both for pyrrole and aniline. It is identical to the theory that the Lewis acid BFEE with good electrophilic property would strongly catalyze the deprotonation of aromatic monomers on the electrodes, resulting in lower oxidation potential [27]. The anodic polarization curves became a key approach to determine the applied potential and to avoid the overoxidation that could result in destruction of the conjugated structure of the polymers and degradation of their properties during the electropolymerization. As time went on, the PPY and PANI nanofilms were deposited on the electrodes, and the as-formed films were used for the subsequent characterizations.

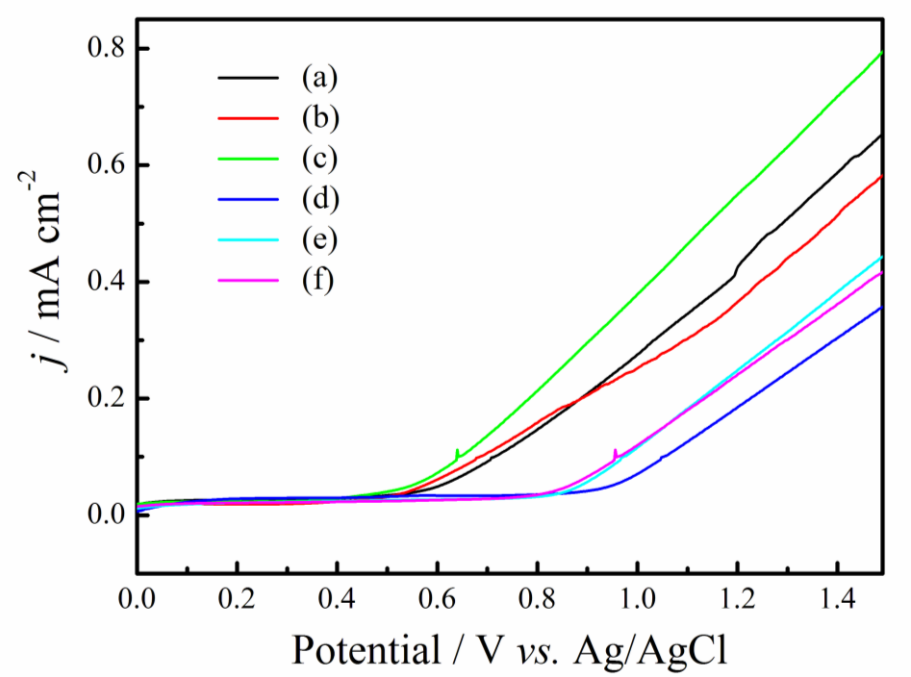

Figure 1. Anodic polarization curves of the monomers in IPA, BFEE, PEG solution with different BFEE contents: (a) 0.025 M pyrrole, 10 % BFEE, (b) 0.025 M pyrrole, 20 % BFEE, (c) 0.025 M pyrrole, 30 % BFEE, (d) 0.05 M aniline, 10 % BFEE, (e) 0.05 M aniline, 20 % BFEE, (f) 0.05 M aniline, 30 % BFEE. The potential scanning rate was 50 mV s^{-1}. *j* denotes the current density.

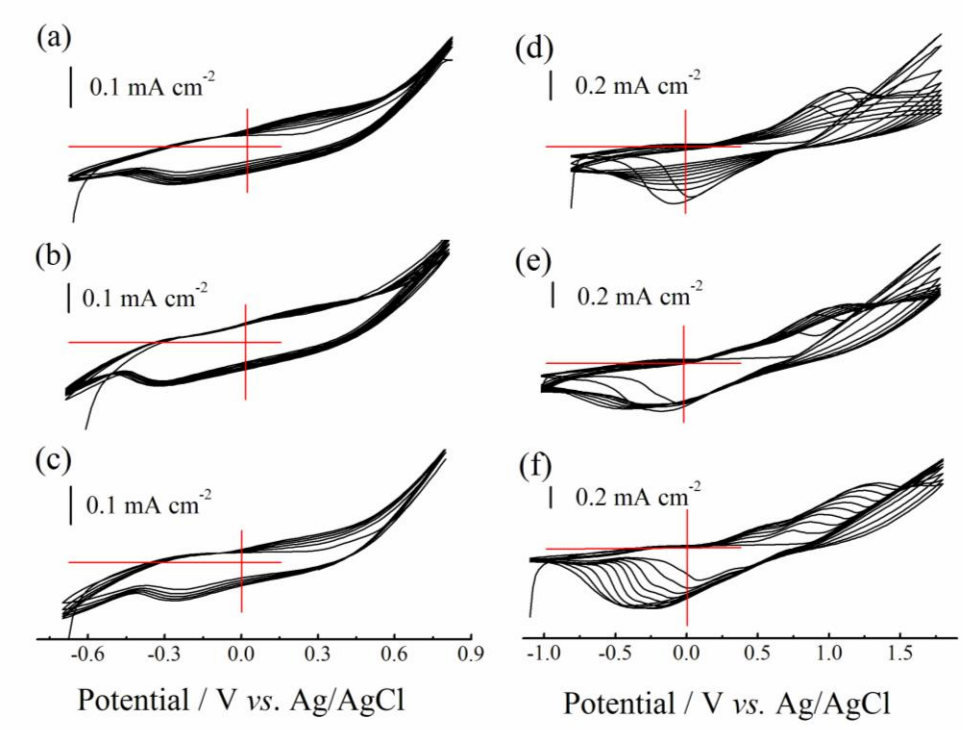

Figure 2. CVs of the monomers in IPA, BFEE, PEG solution with different BFEE contents: Samples a-f. Potential scanning rate: 50 mV s^{-1}.

Successive cyclic voltammograms (CVs) of the anodic electropolymerization of all the films were carried out in a mix system containing the corresponding monomers. The representative electrochemical growth revealing the electrochemical properties of monomers and the formation of corresponding polymers are given in Fig. 2. The oxidation and reduction peaks were distinctly observed for PEDOT:PSS/PPY (a−c) and PEDOT:PSS/PANI films (d−f). The increases of the redox wave currents implied that the amount of the electrodeposited polymer increased on PEDOT:PSS nanofilm electrode with CV proceeding [28]. All these phenomena indicated that conducting nanofilms of PPY and PANI were formed on the PEDOT:PSS nanofilm electrodes.

As listed in Table 1, the thickness of PEDOT:PSS/PPY bilayered nanofilms prepared by electropolymerization is 214.3, 238.3, and 211.8 nm, the thickness of PEDOT:PSS/PANI is 109.0, 108.4, and 109.1 nm. The thickness of spin-coated PEDOT:PSS nanofilms is determined to be 99 nm. It is identified that the PPY and PANI films have been successfully deposited on PEDOT:PSS electrodes, and the thickness of the above layer of PPY and PANI film is in the range of 112.8~139.3 nm and 9.4~10 nm, respectively.

Table 1. Thickness of PEDOT:PSS/PPY and PEDOT:PSS/PANI nanofilms.

	Film thickness (nm)		
Samples	10 % BFEE	20 % BFEE	30 % BFEE
PEDOT:PSS/PPy	214.3	238.3	211.8
PEDOT:PSS/PANI	109.0	108.4	109.1

The electrochemical behaviors of the as-formed nanofilms were determined carefully by CVs in the monomer-free solution of IPA, BFEE, and PEG. As shown in Fig. 3, the redox current density increases when the scan rate increases in the sequence of 25, 50, 100, 150, 200 and 250 mV s^{-1} under each condition. In addition, the peak current densities were proportional to the potential scan rates (the inset of Fig. 4a−f), on one hand, it demonstrated that the electroactive polymers were well adhered to the working electrode surface, on the other hand, it suggested that the redox process is a surface-confined process [29,30] Furthermore, these polymer nanofilms could be repeatedly cycled between the conducting (oxidized) and insulating (neutral) states without significant decomposition, indicating the good stability of PEDOT:PSS/PPY and PEDOT:PSS/PANI films.

Chemical structures of all the films have been investigated by FT-IR and UV-vis spectra. The FT-IR spectra of PEDOT:PSS/PPY and PEDOT:PSS/PANI films are shown in Fig. 4. The inset refers to PEDOT:PSS nanofilms, the vibrations at 1325 and 1515 cm^{-1} are caused by the C−C and C=C stretching of the quinoidal structure and the ring stretching of the thiophene ring of PEDOT chains. The band at about 835 cm^{-1} is related to the C−S bond vibration in the thiophene ring [31]. In the case of PEDOT:PSS/PPY films (Fig. 5a−c), the spectra of the samples show very similar absorption bands. The broad band observed at 3363 cm^{-1} is attributed to the N–H stretching vibration for the nitrogens in the pyrrole rings [32]. The asymmetric and symmetric stretching modes of the pyrrole rings absorb at 1653 and 1430 cm^{-1}.

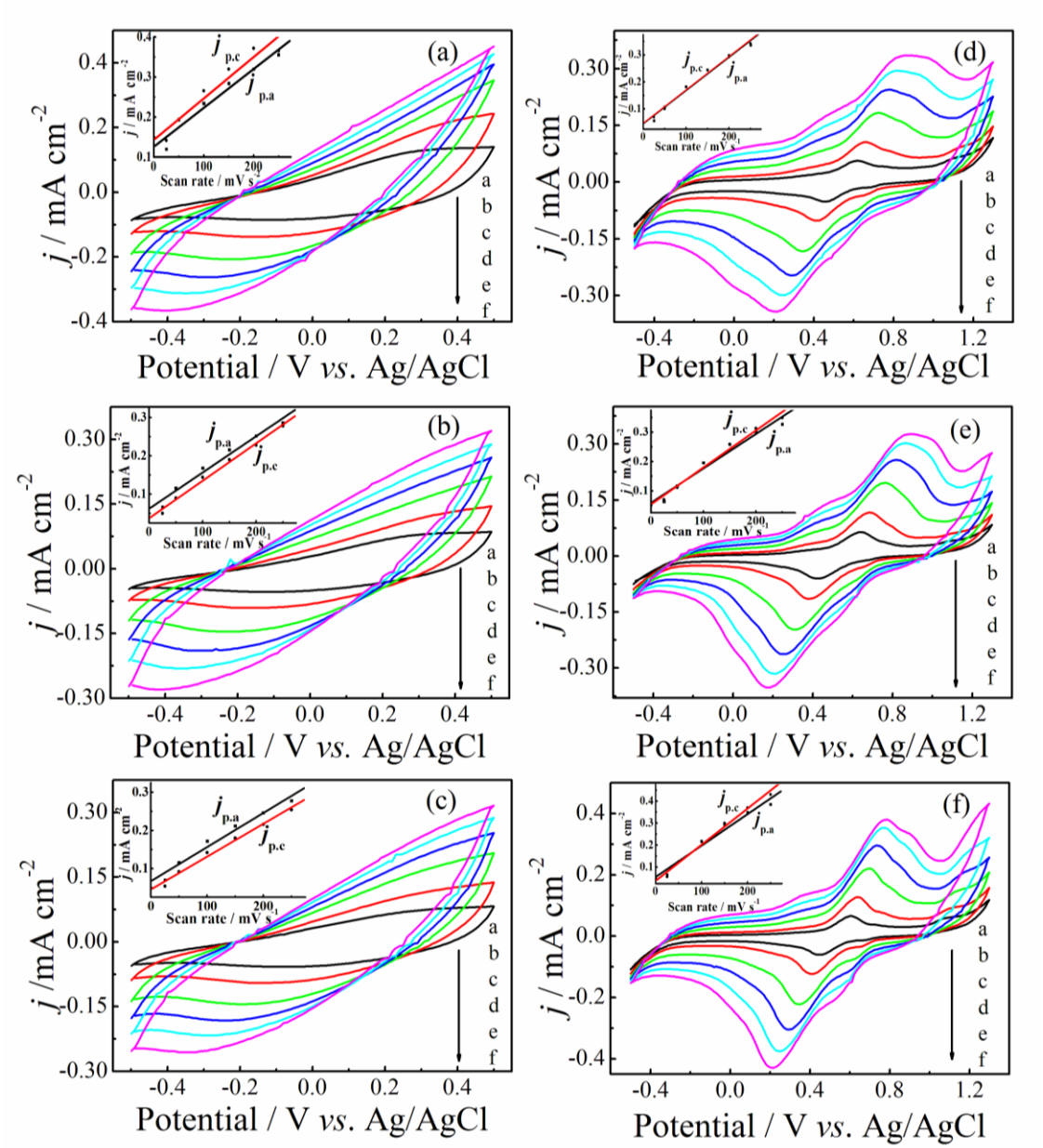

Figure 3. CVs of Samples a−f recorded in the monomer-free mixed solution of IPA, BFEE, and PEG at different potential scan rates: a to f refer to 25, 50, 100, 150, 200, 250 mV s^{-1}. *j* is the current density, and $j_{p.a}$ and $j_{p.c}$ denote the anodic and cathodic peak current densities, respectively.

The characteristic band of C–H deformation vibration appears at 1030 cm^{-1}. The absorption peak at 910 cm^{-1} can be assigned to the C–H deformation vibration in the –CH=CH– group [33]. The spectra of PEDOT:PSS/PANI (Fig. 5d−f) exhibit absorption peaks corresponding to the stretching of quinonoid and benzenoid rings at 1647 cm^{-1} and 1432 cm^{-1}. The N−H stretching is located in 3219 cm^{-1} [34]. The absorption at 1030 cm^{-1} corresponds to the C−H deformation vibration [35]. These results are in good agreement with previous spectroscopic characterizations.

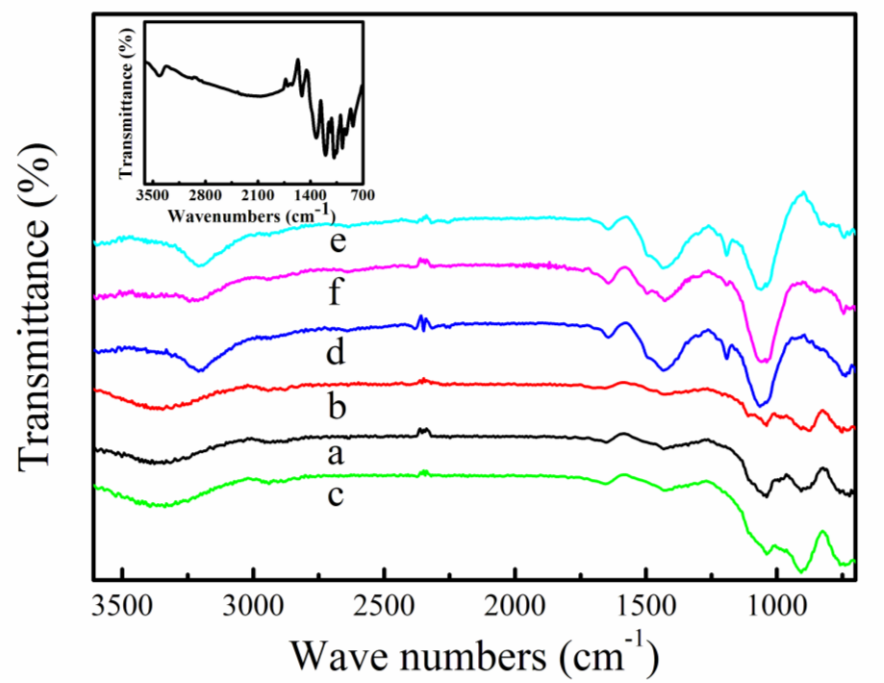

Figure 4. FT-IR spectra of the samples: a−f. The inset refers to PEDOT:PSS nanofilms.

The UV-vis spectra of PEDOT:PSS/PPY and PEDOT:PSS/PANI films are shown in Fig. 5. The measurements were carried out at room temperature in the wavelength range from 300 to 800 nm.

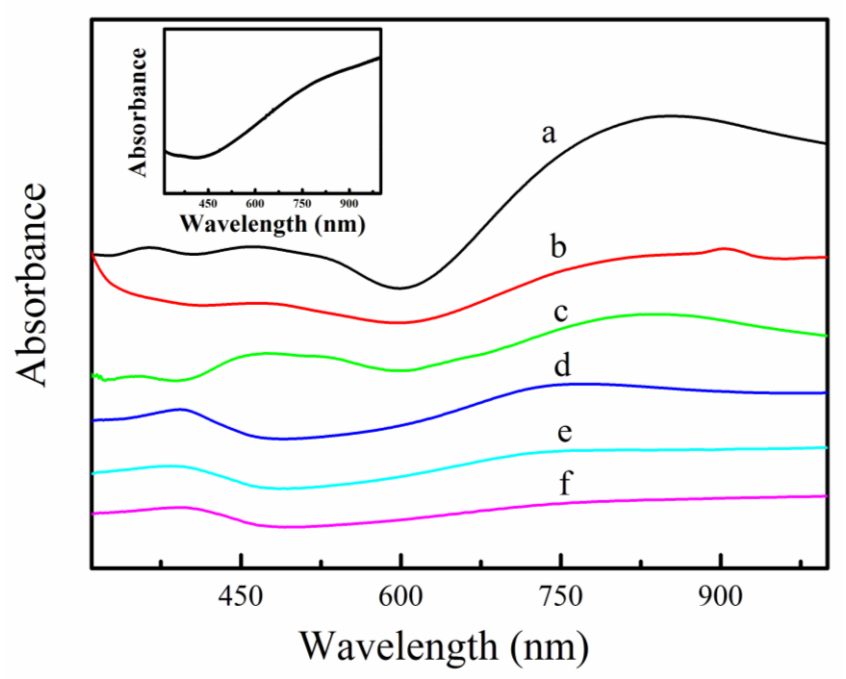

Figure 5. UV-vis absorption spectra of the samples: a−f. The inset refers to PEDOT:PSS nanofilms.

The inset refers to PEDOT:PSS films, which possess an increasing absorption after 500 nm [36]. As for the PEDOT:PSS/PPY films (Fig. 6a−c), broad peak observed from 400 to 585 nm related

to π−π* transitions. The band ranging from 615 to 1000 nm corresponds to the band gap energy between the valence band and the bipolaron band [37,38]. While shown in Fig. 6d−f, the band observed at 405 nm is assigned to the polaron to π* transition, the broad band ranging from 538 to 1000 nm signifies the presence of bipolarons and possibly quinoid structures in PANI [39,40].

Fig. 6 presents the surface SEM image of PPY and PANI films deposited on PEDOT:PSS nanofilm electrodes. The inset refers to the PEDOT:PSS nanofilm electrodes, which are homogeneous, continuous in shape with a smooth surface. For the surface of the PEDOT:PSS/PPY formed with BFEE content of 10% (a), granular PPy was deposited on PEDOT:PSS films [41]. The film appeared to be more densely packed when the content increased to be 20~30% (b, c). The surface of PEDOT:PSS/PANI films prepared with 10% BFEE (d) exhibited the ordered nanotube network structures [42]. When the content increased to be 20% (e), it exhibited particle-packing morphology. The arrangements became more compact for the case of 30% BFEE (f).

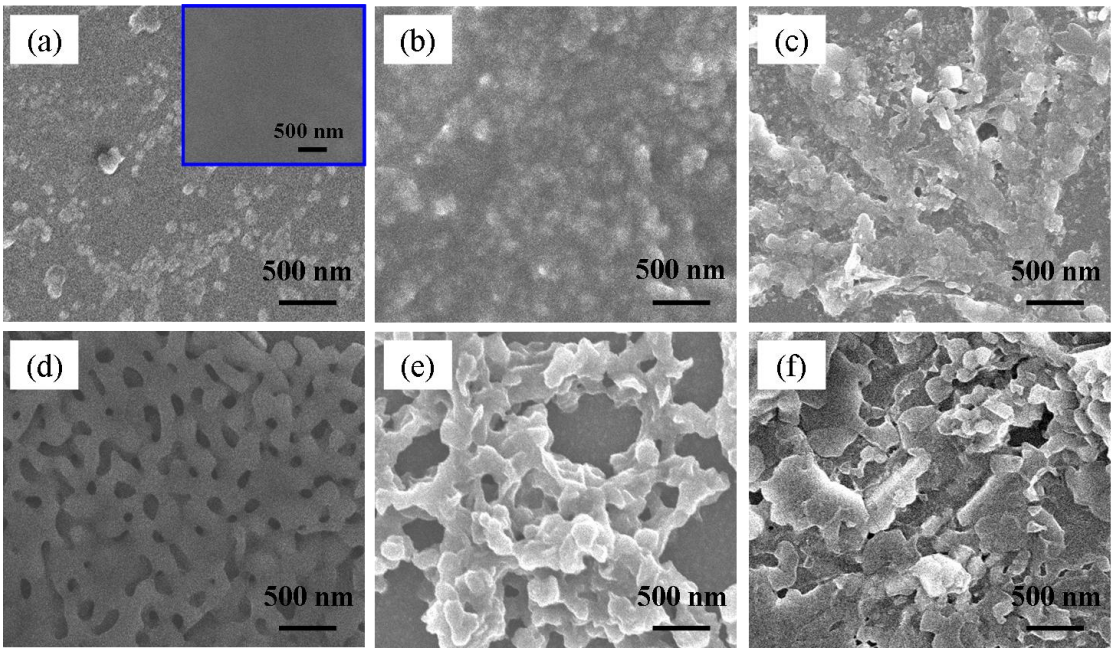

Figure 6. SEM images of the samples: a−f. The inset refers to PEDOT:PSS nanofilm electrodes.

The electrical conductivity and Seebeck coefficient, the two main parameters related to the TE performance, have also been carefully investigated. As for the PEDOT:PSS nanofilms, they possess the electrical conductivity of 393 S cm^{-1}. As listed in Table 2, the room-temperature electrical conductivity of PEDOT:PSS/PPY films was found to be 36.1, 89.8, and 97.1 S cm^{-1} for BFEE content of 10%, 20%, and 30% (Fig. 8a−c). It could be seen that PEDOT:PSS/PPY films with higher electrical conductivity were obtained from the BFEE content of 20~30% [25]. Meanwhile, the values for PEDOT:PSS/PANI films were 136.3, 155.9, and 212.6 S cm^{-1} with 10%, 20%, and 30% BFEE (Fig. 8d−f), which was much larger than the values reported previous: 5.3×10^{-4}, 7.5×10^{-2}, and 0.21 S cm^{-1} [14,43,44]. It has been reported that the substrate contribution to the electrical resistivity is considered negligible when the resistivity ratio between substrate and film is lager than 10000:1 [45]. However,

the electrical resistivity of PEDOT:PSS-glass substrate and PPY (or PANI) films are almost in the same order of magnitude. Thus, it is considered that the high-conductive layer of PEDOT:PSS is beneficial for the electrical conductivity enhancement of the bilayered nanofilms. In addition, with the decrease of the temperature from 300 to 100 K, the electrical conductivity decreases gradually, indicating a typical semiconductor behavior, as shown in Fig. 7.

Table 3. The electrical conductivity, Seebeck coefficient, and power factor of PEDOT:PSS/PPY and PEDOT:PSS/PANI at room temperature.

	PEDOT:PSS/PPy			PEDOT:PSS/PANI		
Samples	10%BFEE	20%BFEE	30%BFEE	10%BFEE	20%BFEE	30%BFEE
σ (S cm^{-1})	36.1	89.8	97.1	136.3	155.9	212.6
S (μV K^{-1})	23.3	20.8	22.3	23.5	27.8	18.7
P (μW m^{-1} K^{-2})	1.96	3.88	4.83	7.53	12.0	7.43

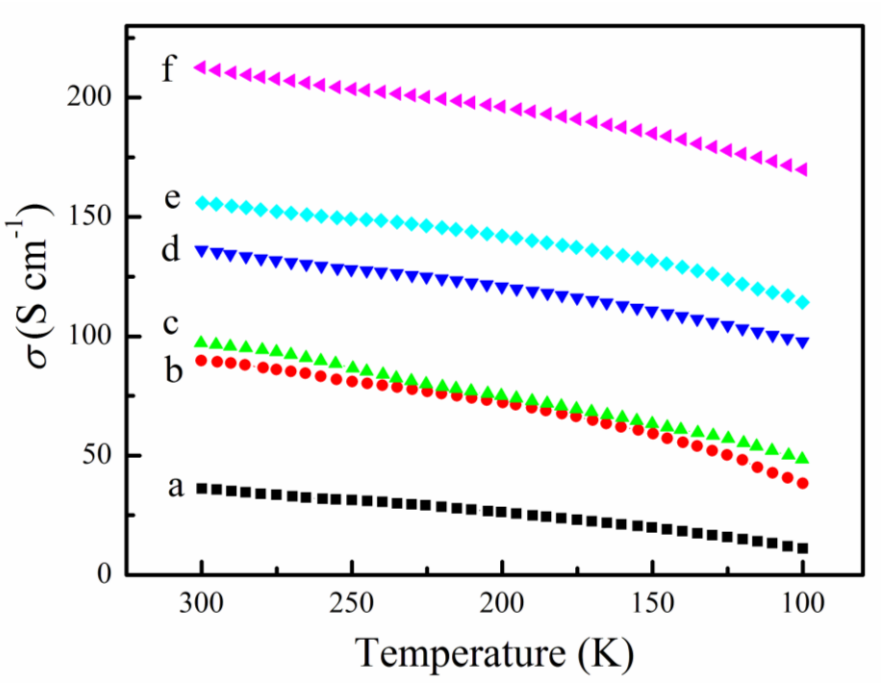

Figure 7. Temperature dependence of the electrical conductivity of the samples: a−f.

As for many conducting polymers, the electrical conductivity follows a quasi one-dimensional (1D) variable range hopping (VRH) model, which is defined as: [16]

$$\sigma(T) = \sigma_0 \exp\left[-\left(\frac{T_0}{T}\right)^{1/2}\right] \quad (1)$$

Where the slope of σ and T_0 can be interpreted as an effective energy separation between localized states due to disorder, and can be described as:

$$T_0 = \frac{16}{\left[K_B N(E_F) L_{\parallel} L_{\perp}^{2}\right]} \qquad (2)$$

Where $N(E_F)$ stands for the density of states at the Fermi level, and $L_{\parallel}(L_{\perp})$ is the localization length in the parallel (perpendicular) direction.

As represented in Fig. 8, it is found that the PEDOT:PSS/PPY and PEDOT:PSS/PANI samples obtained here follows the power law, as in the case of some other conducting polymers [17,18].

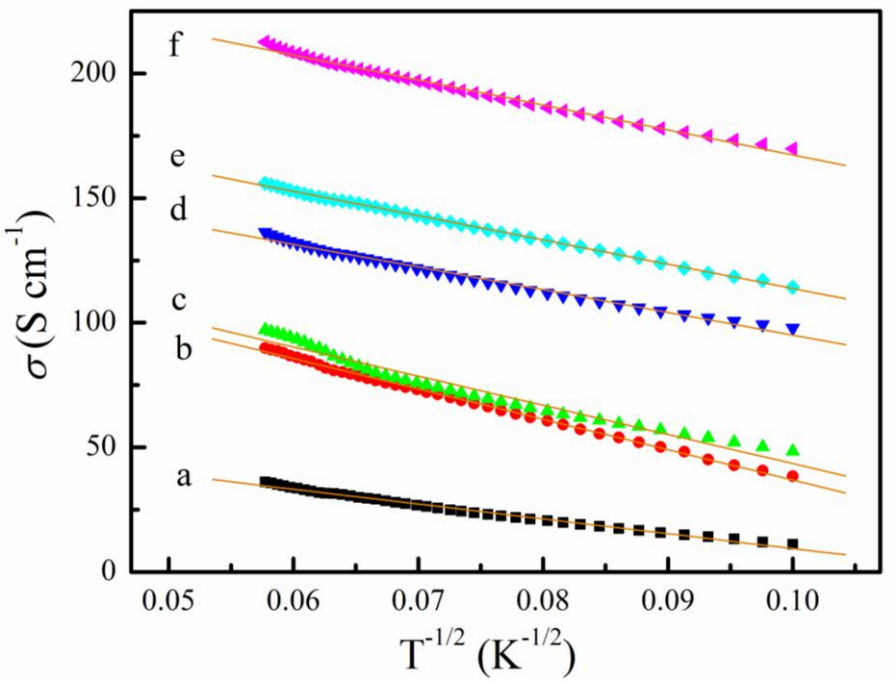

Figure 8. Plot of the electrical conductivity (σ) vs. $T^{-1/2}$ for samples a-f.

Hall measurements were carried out for further evaluation of the electrical conductivity. It is well known that the electrical conductivity of p-type semiconductor can be given by $\sigma = e\mu n$, where e, μ, n are electric charge, carrier mobility, carrier concentration, respectively. The carrier mobility and concentration for PEDOT:PSS films were 0.017 $cm^2\ V^{-1}\ s^{-1}$ and 4.62×10^{22} cm^{-3}. For the BFEE content of 10%, 20%, and 30%, PEDOT:PSS/PPY films possessed the carrier mobility of 3.80, 7.84, and 12.86 $cm^2\ V^{-1}\ s^{-1}$, while the values for PEDOT:PSS/PANI films were 0.016, 0.042, and 0.092 $cm^2\ V^{-1}\ s^{-1}$, respectively.

Table 3. Characteristic carrier mobility, and carrier concentration at room temperature for PEDOT:PSS/PPY and PEDOT:PSS/PANI nanofilms.

	Carrier mobility ($cm^2\ V^{-1}\ s^{-1}$)			concentration (cm^{-3})		
Samples	10%BFEE	20%BFEE	30%BFEE	10%BFEE	20%BFEE	30%BFEE
PEDOT:PSS/PPy	3.80	7.84	12.86	6.01×10^{19}	5.89×10^{19}	4.25×10^{19}
PEDOT:PSS/PANI	0.016	0.042	0.092	1.83×10^{22}	1.10×10^{22}	6.37×10^{21}

It demonstrated that the carrier mobility of PEDOT:PSS/PPy was larger than that of PEDOT:PSS/PANI, which was in good agreement with the previous reports [15,46]. As shown in Table 3, unlike the carrier mobility, the values of the carrier concentrate of PEDOT:PSS/PPY (or PANI) were close to each other. It indicates that the increase of electrical conductivity is mainly due to the increasing carrier mobility.

The Seebeck coefficient is the open-circuit voltage obtained between the two ends of a material subject to a temperature gradient, which usually defined as $S = \Delta V/\Delta T$. Fig. 9 displays the temperature dependence on the Seebeck coefficient for the samples. The Seebeck coefficient of the samples decreases with decreasing temperature from 300 to 250 K, relating to the behavior of organic semiconductor. The positive Seebeck coefficient values suggest the dominant contribution of hole carriers. At 300 K, the Seebeck coefficient of PEDOT:PSS/PPY films was 23.3, 20.8, and 22.3 μV K^{-1} for electropolymerization condition of 10%, 20%, and 30% BFEE (a−c), which was larger than the values in the previous literatures [13,47]. While for PEDOT:PSS/PANI films, the values were 23.5, 27.8, 18.7 μV K^{-1} for BFEE proportion of 10%, 20%, 30%, respectively (d−f), several times larger than the previous reports about 5 μV K^{-1} [14,48] It was encouraging to find out that the Seebeck coefficient values of the bilayered nanofilms were also improved compared with that of PEDOT:PSS nanofilms (15 μV K^{-1}). The improvement was in well consistent with the theoretical calculation [49]. Besides, researchers have investigated the TE performance of the multilayered nanostructures and explained that the reason for the high Seebeck coefficient was because the band edge for the Mott insulator moves continuously with the chemical potential mismatch [50,51]. Meanwhile, Gao et al. considered that the Seebeck coefficient was strongly dependent on the density of states of the bands only close to the Fermi surface since these bands are weighted heavily by the derivative of the Fermi function, and it is the high density of states near the Fermi level that results in the high Seebeck coefficient [52].

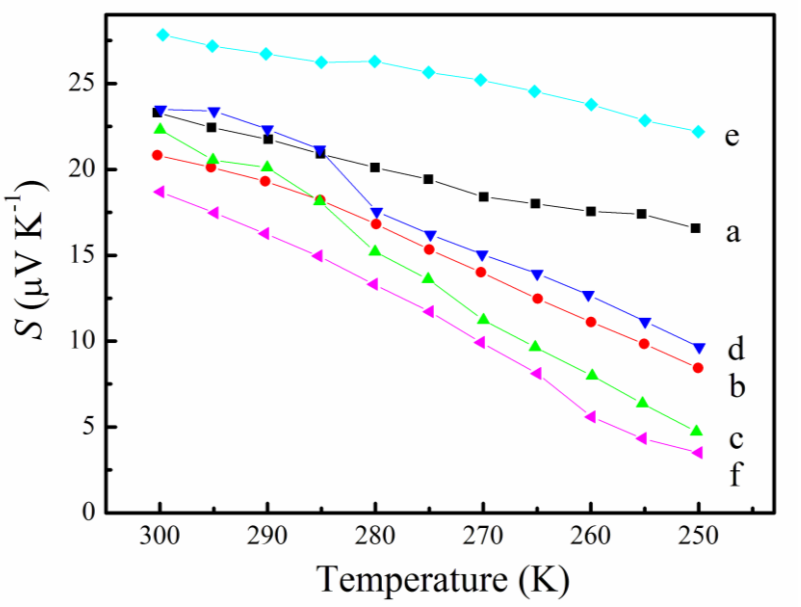

Figure 9. Temperature dependence of the Seebeck coefficient of the samples: a−f.

Fig. 10 shows the variation of the power factor with temperature for all the samples. As for PEDOT:PSS/PPY films, a relatively high power factor of 4.83 μW m^{-1} K^{-2} (sample c, 30% BFEE) was obtained, due to the relatively high electrical conductivity, the *ZT* value was 1.45×10^{-3} when the thermal conductivity was 1.0 W m^{-1} K^{-1} by estimates [53]. While for PEDOT:PSS/PANI films, the maximum power factor could reach up to 12.0 μW m^{-1} K^{-2} (sample e, 20% BFEE) for the high Seebeck coefficient of 27.8 μW m^{-1} K^{-2}. The maximum *ZT* value was 2.12×10^{-2} when referencing the literature thermal conductivity value of 0.17 W m^{-1} K^{-1} [54], two orders of magnitude larger than the previous report [2]. It is expected that the developed synthesis strategy is powerful and general, and can be easily extended to fabricate other multilayered nanostructures by simply choosing different conducting polymers such as polycarbazole (PCZ) and its derivatives, providing more potential for future application in TE devices.

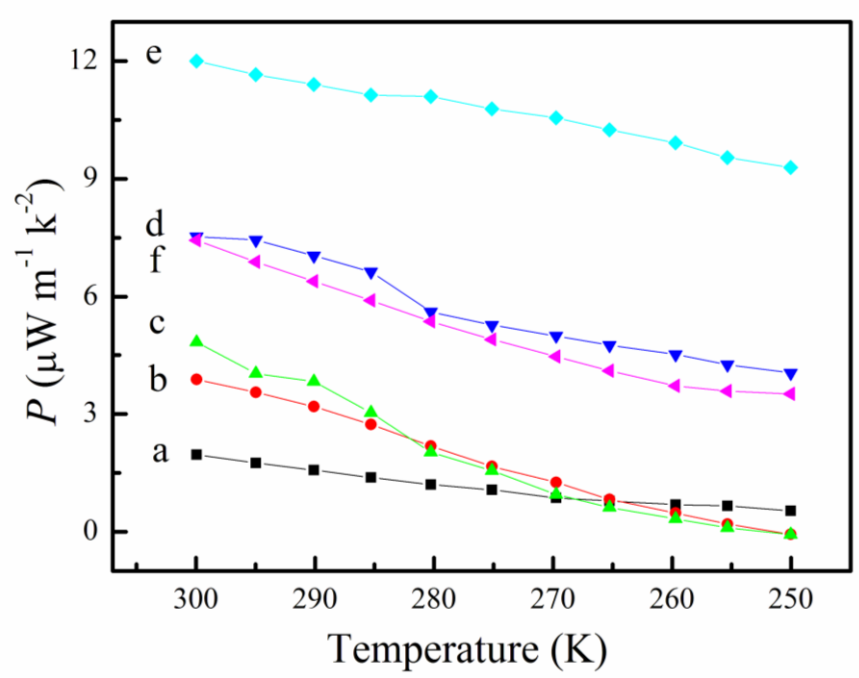

Figure 10. Temperature dependence of the power factor of the samples: a−f.

4. CONCLUSIONS

In summary, a novel generation of bilayered nanofilms of PEDOT:PSS/PPY and PEDOT:PSS/PANI with enhanced TE performance were electrochemical fabricated successfully. The maximum Seebeck coefficient value was 23.3 μV K^{-1} for PEDOT:PSS/PPY and 27.8 μV K^{-1} for PEDOT:PSS/PANI, larger than that of PEDOT:PSS, PPY, and PANI. The maximum power factor of PEDOT:PSS/PANI films could reach up to be 12.0 μW m^{-1} K^{-2}, achieving the corresponding *ZT* value of 2.12×10^{-2} by estimates, improved by two orders of magnitude. The results indicated that it may mainly due to the high density of states near the Fermi level that results in the high Seebeck

coefficient, thus, realizing the enhancement in the *ZT* value. Most important of all, the approach may potentially be extended to other material systems and provide a facile and general strategy to achieve better TE properties, paving the way for applications in thermoelectric or other organic electronics devices.

ACKNOWLEDGEMENTS
This work was supported by National Natural Science Foundation of China (51463008, 51203070, 51303073), Jiangxi Provincial Department of Education (GJJ13565), Jiangxi Provincial Department of Science and Technology (20142BAB216032), and Training Plan for the Main Subject of Academic Leaders of Jiangxi Province.

References

1. Q. Zhang, T. Sun, F. Cao, M. Li, M.H. Hong, J.K. Yuan, Q.Y. Yan, H.H. Hng, N.Q. Wu, X.G. Liu, *Nanoscale* 2 (2010) 1256.
2. N. Toshima, *Macromol. Symp.* 186 (2002) 81.
3. M.S. Dresselhaus, G. Chen, M.Y. Tang, R.G. Yang, H. Lee, D.Z. Wang, Z.F. Ren, J.P. Fleurial, P. Gogna, *Adv. Mater.* 19 (2007) 1043.
4. B. Poudel, Q. Hao, Y. Ma, Y.C. Lan, A. Minnich, B. Yu, X. Yan, D.Z. Wang, A. Muto, D. Vashaee, X.Y. Chen, J.M. Liu, M.S. Dresselhaus, G. Chen, Z.F. Ren, *Science* 320 (2008) 634.
5. O. Bubnova, Z.U. Khan, A. Malti, S. Braun, M. Fahlman, M. Berggren, X. Crispin, *Nat. Mater.* 10 (2011) 429.
6. G.H. Kim, L. Shao, K. Zhang, K.P. Pipe, *Nat. Mater.* 12 (2013) 719.
7. S. Teehan, H. Efstathiadis, P. Haldar, *J. Alloys Compd.* 539 (2012) 129.
8. H.J. Song, C.C. Liu, J.K. Xu, Q.L. Jiang, H. Shi, *RSC Adv.* 3 (2013) 22065.
9. L.F. Lai, L. Wang, H.P. Yang, N.G. Sahoo, Q.X. Tam, J.L. Liu, C.K. Poh, S.H. Lim, Z.X. Shen, J.Y. Lin, *Nano Energy* 1 (2012) 723.
10. S. Jussila, M. Puustinen, T. Hassinen, J. Olkkonen, H.G.O. Sandberg, K. Solehmainen, *Org. Electron.* 13 (2012) 1308.
11. S.J. Peng, L.L. Tian, J. Liang, S.G. Mhaisalkar, S. Ramakrishna, *ACS Appl. Mater. Interfaces* 4 (2012) 397.
12. Y.X. Li, X.J. Hu, S.Y. Zhou, L. Yang, J. Yan, C.H. Sun, P. Chen, *J. Mater. Chem. C* 2 (2014) 916.
13. D.S. Maddison, J. Unsworth, *Synth. Met.* 26 (1988) 99.
14. F. Yakuphanoglu, B.F. Şenkal, *J. Phys. Chem. C* 111 (2007) 1840.
15. Q. Yao, L.D. Chen, W.Q. Zhang, S.C. Liufu, X.H. Chen, *ACS Nano* 4 (2010) 2445.
16. N.F. Mott, E. Davis, *Electronic Process in Non-Crystalline Materials*, Clarendon Press, Oxford, 1979, and references therein.
17. F. Zuo, M. Angelopoulos, A.G. MacDiarmid, A.J. Epstein, *Phys. Rev. B* 36 (1987) 3475.
18. J. Joo, S.M. Long, J.P. Pouget, E.J. Oh, A.G. MacDiarmid, A.J. Epstein, *Phys. Rev. B* 57 (1998) 9567.
19. A.J. Epstein, W.P. Lee, V.N. Prigodin, *Synth. Met.* 117 (2001) 9.
20. K. Sun, Y.J. Xia, J.Y. Ouyang, *Sol. Energy Mater. Sol. Cells* 97 (2012) 89.
21. Y.J. Xia, K. Sun, J.Y. Ouyang, *Energy Environ. Sci.* 5 (2012) 5325.
22. L. Groenendaal, F. Jonas, D. Freitag, H. Pielartzik, J.R. Reynolds, *Adv. Mater.* 12 (2000) 481.
23. J.K. Kim, W. Kim, D.H. Wang, H. Lee, S.M. Cho, D. Choi, J.H. Park, *Langmuir* 29 (2013) 5377.
24. H. Shi, C.C. Liu, J.K. Xu, H.J. Song, B.Y. Lu, F.X. Jiang, W.Q. Zhou, G. Zhang, Q.L. Jiang, *ACS Appl. Mater. Interfaces* 5 (2013) 12811.

25. J.K. Xu, G.Q. Shi, L.T. Qu, J.X. Zhang, *Synth. Met.* 135–136 (2003) 221.
26. D. Kim, Y. Kim, K. Choi, J.C. Grunlan, C. Yu, *ACS Nano* 4 (2010) 513.
27. G.Q. Shi, S. Jin, G. Xue, C. Li, *Science* 267 (1995) 994–996.
28. C.C. Liu, B.Y. Lu, C.L. Fan, J.K. Xu, Y.Z. Li, F.X. Jiang, *J. Solid State Electrochem.* 14 (2010) 1153.
29. G. Sönmez, I. Schwendeman, P. Schottland, K, Zong, J.R. Reynolds, *Macromolecules* 36 (2003) 639.
30. A.E.F. Nassar, Z. Zhang, N. Yu, J.F. Rusling, T.F. Kumosinski, *J. Phys. Chem. B* 101 (1997) 2224.
31. J.M. Jian, X.S. Guo, L.W. Lin, Q. Cai, J. Cheng, J.P. Li, *Sens. Actuators, B* 178 (2013) 279.
32. L. Liu, C.J. Zhao, Y.M. Zhao, N.Q. Jia, Q. Zhou, M.M. Yan, Z.Y. Jiang, *Eur. Polym. J.* 41 (2005) 2117.
33. G.J. Qi, Z.L. Wu, H.L. Wang, *J. Mater. Chem. C* 1 (2013) 7102.
34. S.K. Pillalamarri, F.D. Blum, A.T. Tokuhiro, M.F. Bertino, *Chem. Mater.* 17 (2005) 5941.
35. H. Gomez, M.K. Ram, F. Alvi, E. Stefanakos, A. Kumar, *J. Phys. Chem. C* 114 (2010) 18797.
36. J.Y. Ouyang, Q.F. Xu, C.W. Chu, Y. Yang, G. Li, J. Shinar, *Polymer* 45 (2004) 8443.
37. S.T. Selvan, T. Hayakawa, M. Nogami, M. Möller, *J. Phys. Chem. B* 103 (1999) 7441.
38. K.E. Hnida, R.P. Socha, G.D. Sulka, *J. Phys. Chem. C* 117 (2013) 19382.
39. Y.N. Xia, J.M. Wiesinger, A.G. MacDiarmid, A.J. Epstein, *Chem. Mater.* 7 (1995) 443.
40. P. Olejnik, M. Gniadek, B. Palys, *J. Phys. Chem. C* 116 (2012) 10424.
41. G.P. Zhang, H.H. Zhou, J.L. Zhang, X. Han, J.H. Chen, Y.F. Kuang, *J. Appl. Polym. Sci.* 125 (2012) 2342.
42. H.W. Park, T. Kim, J. Huh, M. Kang, J.E. Lee, H. Yoon, *ACS Nano* 6 (2012) 7624.
43. H. Devendrappa, U.V.S. Rao, M.V.N.A. Prasad, *J. Power Sources* 155 (2006) 368.
44. S. Palaniappan, *Polym. Adv. Technol.* 13 (2002) 54.
45. M.O. Manasreh, T.H. Myers, F.H. Julien, *Infrared applications of semiconductors-materials, processing and devices*, 2nd ed.; A.V. Wagner, R.J. Foreman, J.C. Farmer, T.C. Barbee, Eds.; Materials Research Society: Pittsburgh, 1996; p 467–472.
46. S. Patwardhan, A.A. Kocherzhenko, F.C. Grozema, L.D.A. Siebbeles, *J. Phys. Chem. C* 115 (2011) 11768.
47. T. Stöcker, A. Köhler, R. Moos, *J. Polym. Sci. B: Polym. Phys.* 50 (2012) 976.
48. R.B. Aïch, N. Blouin, A. Bouchard, M. Leclerc, *Chem. Mater.* 21 (2009) 751.
49. R. Kim, M.S. Lundstrom, *J. Appl. Phys.* 110 (2011) 034511.
50. J.K. Freericks, V. Zlatić, *Phys. Stat. Sol. B* 244 (2007) 2351.
51. H. Fritzsche, *Solid State Commun.* 9 (1971) 1813.
52. X. Gao, K. Uehara, D.D. Klug, S. Patchkovskii, J.S. Tse, T.M. Tritt, *Phys. Rew. B* 72 (2005) 125202.
53. B.A. Lunn, J. Unsworth, N.G. Booth, P.C. Innis, *J. Mater. Sci.* 28 (1993) 5092.
54. H. Yan, N. Ohno, N. Toshima, *Chem. Lett.* 29 (2002) 392.